

Optics Letters

Nonlinear Raman–Nath diffraction of femtosecond laser pulses in a 2D nonlinear photonic crystal

A. M. VYUNISHEV,^{1,2,*} V. G. ARKHIPKIN,^{1,3} V. V. SLABKO,² I. S. BATURIN,^{4,5}
A. R. AKHMATKHANOV,^{4,5} V. YA. SHUR,^{4,5} AND A. S. CHIRKIN⁶

¹L.V. Kirensky Institute of Physics, Krasnoyarsk 660036, Russia

²Department of Photonics and Laser Technology, Siberian Federal University, Krasnoyarsk 660079, Russia

³Laboratory for Nonlinear Optics and Spectroscopy, Siberian Federal University, Krasnoyarsk 660079, Russia

⁴Ural Federal University, Ekaterinburg 620000, Russia

⁵Labfer Ltd., Ekaterinburg 620014, Russia

⁶Faculty of Physics and International Laser Center, M. V. Lomonosov Moscow State University, Moscow 119992, Russia

*Corresponding author: vyunishev@iph.krasn.ru

Received 24 June 2015; revised 27 July 2015; accepted 27 July 2015; posted 27 July 2015 (Doc. ID 243548); published 20 August 2015

We study second-harmonic generation (SHG) of femtosecond laser pulses in a rectangular two-dimensional nonlinear photonic crystal (NLPC). Multiple SH beams were observed in the vicinity of the propagation direction of the fundamental beam. It has been verified that the angular positions of these beams obey the conditions of nonlinear Raman–Nath diffraction (NRND). The measured SH spectra of specific NRND orders consist of narrow peaks that experience a high-frequency spectral shift as the order grows. We derive an analytical expression for the process studied and find the theoretical results to be in good agreement with the experimental data. We estimate the enhancement factor of nonlinear Raman–Nath diffraction in 2D NLPC to be 70. © 2015 Optical Society of America

OCIS codes: (190.2620) Harmonic generation and mixing; (190.4223) Nonlinear wave mixing; (190.4420) Nonlinear optics, transverse effects in.

<http://dx.doi.org/10.1364/OL.40.004002>

Nonlinear frequency conversion in two-dimensional (2D) nonlinear photonic crystals (NLPCs) has been the subject of numerous studies [1–16] since the concept of NLPC was proposed [1]. These crystals enable a variety of noncollinear nonlinear processes that manifest themselves as sum and difference frequency generation and parametric down conversion. An important advantage of NLPCs originates from spatial modulation of the sign of nonlinear susceptibility providing reciprocal “nonlinear” lattice vectors such that the phase-matching conditions become feasible in three wave-mixing processes. For instance, periodic 2D NLPC are found to be promising media for cascaded frequency conversion via Čerenkov nonlinear diffraction [6], study of the nonlinear Talbot effect [7], and generation of entangled-path biphotons [8]. More complicated spatial realizations of 2D NLPC enable all-optical deflection [9], generation of nondiffracting Airy

beams [10], and twisted photons [11] (see also review [12]). While most of the previous studies on nonlinear frequency conversion in periodic 2D NLPC have essentially focused on spatial characteristics of the generated radiation, the spectral characteristics of this process remain insufficiently studied. It has recently been shown that properly designed 1D NLPC can be used for spectral shaping [13]. This approach can be extended to the case of 2D NLPC to obtain the desired spatial as well as spectral characteristics of the generated radiation. Although some approaches have been developed to calculate SHG in 2D NLPCs, such as the method based on Green’s function formalism [14], the transfer-matrix method [15] and the effective nonlinear coefficient model [16,17], it is desirable to have a simple approach adopted to periodic rectangle 2D NLPCs. Developing this approach is essential for designing 2D NLPCs with required nonlinear optical characteristics.

In this Letter, we report our studies on the second-harmonic generation (SHG) of femtosecond laser pulses in rectangle 2D NLPCs. This process is found to be in close analogy with nonlinear Raman–Nath diffraction, which takes place in 1D nonlinear photonic lattices [18–23]. We derive analytical expression describing SHG under nonlinear Raman–Nath diffraction in rectangle 2D NLPCs. The main advantage of 2D NLPC is the ability of these crystals to enhance the efficiency of SHG due to quasi-phase matching, which provides a tool for spectral shaping of generated radiations.

The sample studied is a congruent lithium niobate crystal having the dimensions $5.0 \times 5.0 \times 0.5 \text{ mm}^3$. The structure of the sample is a two-dimensional rectangular nonlinear photonic lattice with a rectangular motif, where the rectangle-shaped prisms are embedded into a bulk medium with the inverse sign of quadratic nonlinear susceptibility. These prisms stand at the regular lattice points with periodicity $10 \times 115 \mu\text{m}^2$, as sketched in Fig. 1(a). The NLPC structure was fabricated by the electric-field poling procedure [24] (Labfer Ltd). Figure 1(b) shows a polar facet of the sample after the chemical etching procedure. In the experiments,

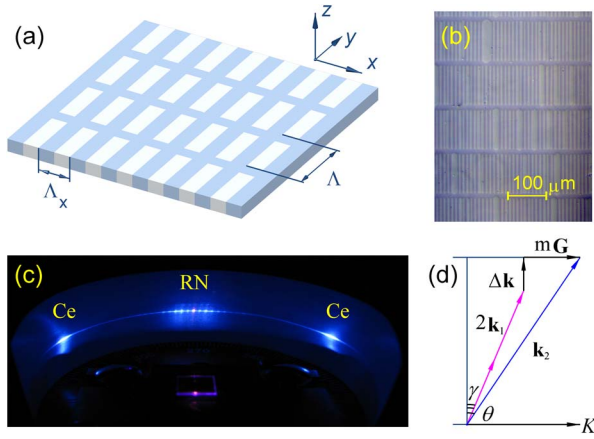


Fig. 1. Design of a 2D nonlinear photonic structure (a), a pattern etched on the polar facet of the crystal (b), and the pattern observed on the screen (c). Peripheral spots correspond to Čerenkov nonlinear diffraction (marked as Ce), and the central spots are nonlinear Raman–Nath diffraction (marked as RN). (d) Phase-matching diagram.

the fundamental frequency (FF) beam from a Ti:sapphire oscillator (Tsunami, Spectra-Physics), delivering 100-fs pulses at a repetition rate of 80 MHz (central wavelength 800 nm), was focused with a 20-cm lens into the sample to produce a beam $w_0 = 80$ micron in focal diameter. The fundamental radiation propagated along the y -axis and its polarization coincided with the z -axis to employ the highest nonlinear coefficient of lithium niobate d_{33} . Figure 1(c) shows the SH pattern observed on a cylindrical screen 3 cm from the center of the sample. Next to the side spots corresponding to Čerenkov nonlinear diffraction [25], one can distinguish a set of ordered SH spots in the vicinity of the passed FF beam. It is believed that the SH beams correspond to the nonlinear Raman–Nath diffraction due to the periodicity of the structure in the transverse direction. A phase-matching diagram is presented in Fig. 1(d). Here \mathbf{k}_1 and \mathbf{k}_2 are the wavevectors of FF and SH, respectively, $\Delta\mathbf{k} = \mathbf{k}_2 - 2\mathbf{k}_1$ is the wave vector mismatch, \mathbf{G} is the primary reciprocal lattice vector, and m is the NRND order. We clearly observe eleven SH beams corresponding to the six orders. The angular positions of SH beams β_m have been proved to obey the NRND condition valid for periodic 1D structures

$$\sin(\beta_m) = m|\mathbf{G}|/|\mathbf{k}_2|. \quad (1)$$

The calculated and measured NRND angles are summarized in Table 1. From the above, we conclude that the NRND also contributes to the SHG in 2D NLPCs. The measured Čerenkov nonlinear diffraction angle is 56.4 deg, which agrees with the calculated value 56.7 deg.

For theoretical analysis of SHG in a 2D structure, we start with the model known for the nonlinear diffraction in a 1D structure [26]. In the low conversion limit, where depletion of the pump can be neglected, the SH Fourier spectrum in a 1D structure of the length L is given by the form

$$A(\Omega, K_X, K_Z, L) = F(\Omega, K_X, K_Z, L)R(K_X) \int_0^L \exp(iQy)dy. \quad (2)$$

We introduce the following designations

Table 1. Predicted and Measured NRND Order Parameters

NRND order	Prediction [deg]	Measurement [deg]	
		Positive	Negative
0	0	$0 \pm 3 \cdot 10^{-3}$	
1	2.292	$2.298 \pm 3 \cdot 10^{-3}$	$2.298 \pm 3 \cdot 10^{-3}$
2	4.589	$4.601 \pm 3 \cdot 10^{-3}$	$4.608 \pm 3 \cdot 10^{-3}$
3	6.892	$6.877 \pm 3 \cdot 10^{-3}$	$6.856 \pm 3 \cdot 10^{-3}$
4	9.207	$9.258 \pm 3 \cdot 10^{-3}$	$9.251 \pm 3 \cdot 10^{-3}$
5	11.537	$11.554 \pm 3 \cdot 10^{-3}$	$11.547 \pm 3 \cdot 10^{-3}$

$$F(\Omega, K_X, K_Z, L) = -i(\pi/2)^{3/2}\beta_2 I_1(0)\tau a^2 \times \exp(-iqL - [(\tau\Omega)^2 + (aK_Z)^2]/8)$$

$$R(K_X) = \sum_m g_m \exp(-a^2(mG + K_X)^2/8)$$

$$q = \Omega/u_2 - K_X^2/2k_2,$$

$$Q = \Delta k + \nu\Omega - (K_X^2 + K_Z^2)/2k_2$$

$$\Delta k = k_2 - 2k_1, \quad \nu = (1/u_2 - 1/u_1),$$

$$\Omega = 2\pi c(1/\lambda_2 - 2/\lambda_0). \quad (3)$$

Here $\beta_2 = 64\pi^3\chi^{(2)2}/(c\lambda_1 n_1 n_2)$ is the nonlinear coupling coefficient, $I_1(0)$ is the FF intensity at the beam center, 2τ and $2a$ are the pulse duration and the focal spot diameter of the FF beam, respectively; Ω is the frequency detuning from the central double frequency, λ_0 is the central FF wavelength and λ_2 is the SH spectral component, K_X, K_Z are the so-called spatial frequencies, Δk is the wavevector mismatch between FF (k_1) and SH (k_2) in the direction y , ν is the group velocity mismatch ($u_{1,2}$ is the group velocity), and g_m is the Fourier coefficients [23], where $m = 0, \pm 1, \pm 2, \dots$

Integration of Eq. (2) gives the SH spectral amplitude generated in a 1D structure of the length d [26]:

$$A(\Omega, K_X, K_Z, d) = F(\Omega, K_X, K_Z, d) \times R(K_X)d \exp(iQd/2)\text{sinc}(Qd/2), \quad (4)$$

where $\text{sinc}(x) = \sin(x)/x$.

The function $R(K_X)$ produces a series of maxima at the spatial frequencies. The relation between the spatial frequency and the internal SH propagation angle can be found geometrically using the phase-matching diagram shown in Fig. 1(d): $K_X = k_2 \sin(\theta) - 2k_1 \sin(\gamma)$, where γ and θ are the inner FF and SH propagation angles. We consider extraordinary waves and use the Sellmeier coefficients from Ref. [27] to approximate refractive indexes of lithium niobate. For the oblique incidence of the FF wave, we can represent the full wavevector mismatch in Eq. (3) as $Q = k_2 \cos(\theta) - 2k_1 \cos(\gamma) + \nu\Omega$ [20].

For a homogeneous nonlinear layer ($g(x) = g^{(0)} = \text{const}$) of the length h we have

$$A(\Omega, K_X, K_Z, h) = F(\Omega, K_X, K_Z, h) \times R^{(h)}(K_X)h \exp(iQh/2)\text{sinc}(Qh/2),$$

$$R^{(h)}(K_X) = g^{(0)} \exp(-(aK_X)^2/8). \quad (5)$$

Let us now treat 2D NLPC as a stack of 1D periodic structures (along the x -axis) spaced by 12 μm in the direction along

the y -axis. The elementary period of NLPC along the y -axis is $\Lambda = 115 \mu\text{m}$; it includes two layers, one being a 1D structure (an inhomogeneous layer of the length d) formed along the x -axis and the other one being a monodomain (homogeneous) layer of the length b ($\Lambda = d + b$). In this case, the total SH spectral amplitude generated in a layered structure is a superposition of the fields generated by each layer, taking into account the phase accumulated along the propagation direction.

It is possible to summarize separately the contributions from inhomogeneous and homogeneous layers to the SH amplitude. As a result, the SH amplitude after N layers is expressed as follows:

$$A(\Omega, K_X, K_Z, L) = F(\Omega, K_X, K_Z, L) \times \exp(iQ(L-b)/2) \times P(Q) \{ dR(K_X) \text{sinc}(Qd/2) + bR^{(b)}(K_X) \exp(iQ\Lambda/2) \text{sinc}(Qb/2) \}, \quad (7)$$

where

$$P(Q) = \sin(QL/2) / \sin(Q\Lambda/2). \quad (8)$$

Factor (8) is similar to the one observed at diffraction of the plane wave on a rectangular amplitude lattice. By means of Eq. (7), we can find the frequency-angle SH spectral intensity $S(\Omega, K_X, K_Z, L) = |A(\Omega, K_X, K_Z, L)|^2$. Factor (8) and the function $R(K_X)$ in Eq. (3) determine the main features of nonlinear diffraction of ultrashort laser pulses in 2D structures. The spectral maxima on the angular distribution take place when $Q\Lambda = 2\pi p$ ($p = 0, \pm 1, \pm 2, \dots$) and $K_X = -mG$. If $K_Z = 0$, then the SH frequency maximum is shifted by $\Omega_{\text{sh}} = (\Delta k - K_X^2/2k_2)/\nu$. According to Eq. (8), the frequency interval between the spectral maxima equals $\Delta\Omega = 2\pi/(|\nu|\Lambda)$ or $\Delta\lambda_2 = \lambda_2^2/(c|\nu|\Lambda)$. The SH frequency spectrum has the width $\delta\lambda_2 \approx \lambda_2^2/(c|\nu|L)$ for all quasi-phase-matching orders. Under our experimental conditions, we have $\delta\lambda_2 \approx 0.06 \text{ nm}$ and $\Delta\lambda_2 = 2.45 \text{ nm}$ ($\nu = 1.89 \cdot 10^{-9} \text{ s} \cdot \text{m}^{-1}$). If $b \ll d$, it is clear from Eq. (7) that functions $R(K_X)$ and $P(Q)$ are responsible for angular and frequency-angle characteristics of SH, respectively. Hence varying parameters of the structure, we can independently manage spatial and spectral characteristics of SH waves.

To measure angular characteristics of SH, a 120- μm -width slit was mounted on a motorized translation stage 50 mm away from the sample. Using a 918D power meter (Newport), we measured the averaged SH power passed through the slit as a function of the slit coordinate in the direction normal to the FF beam. The angular distribution of the SH power is very sensitive to the FF incidence angle onto the sample. In the experiment, the fundamental radiation was directed at a small angle to the y -axis in the XY-plane of the crystal to prevent undesired back reflection to the oscillator. As a result, the measured angular distribution of the SH power is slightly asymmetric as shown in Fig. 2. The relatively high background signal could be a result of the SHG in homogeneous layers [the second term in Eq. (7)], as well as minor imperfection of the nonlinear structure and light scattering at the facets. The SHG efficiency for the central beam determined by $\eta = P_{2\omega}/P_{\omega}^2$ was up to $3 \times 10^{-3}\% \cdot \text{W}^{-1}$.

The spectra of specific SH beams were measured using a MSDD1000 spectrometer (Solar TII, Corp.). As shown in Fig. 3, the SH spectrum for the central SH beam ($m = 0$)

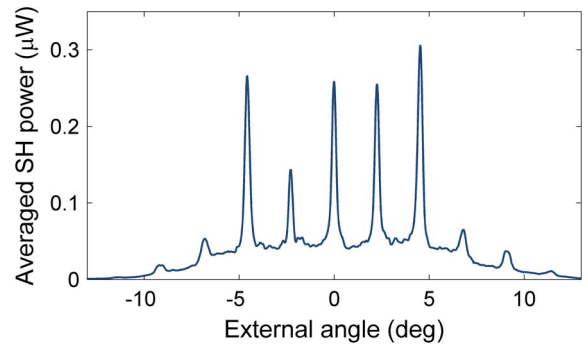


Fig. 2. Measured angular distribution of averaged SH power for FF incidence angle ~ 3 mrad.

consists of narrow peaks. The measured spectral width of the SH maxima and the spectral interval between them are $\delta\lambda_2 \approx 0.2 \text{ nm}$ and $\Delta\lambda_2 = 2.6 \text{ nm}$, respectively. The spectrum calculated using Eq. (7) reproduces the measured one as illustrated in the same graph. These spectra differ from the ones corresponding to SHG in a 1D structure [23]. We believe these peaks to be attributed to the 45th- and 44th-order QPM SHG. Actually, the full wavevector mismatch in the propagation direction for the zero transverse order must be equal to one of the spatial harmonics provided by the structure, i.e., $Q(\lambda_2, m = 0) = p|\mathbf{G}_y| = 2\pi p/\Lambda$. This requirement is fulfilled at the following parameters: $\lambda_2 = 399.6 \text{ nm}$ for $p = 45$ and $\lambda_2 = 402.2 \text{ nm}$ for $p = 44$. Similar spectra were measured for the SH beams for the first five NRND orders as shown in Fig. 4(a). The spectral peaks tend to shift toward shorter wavelength range with increasing NRND order. This tendency is explained by the behavior of the wavevector mismatch in Eq. (7) $Q = \Delta k + \nu\Omega - (mG)^2/2k_2$ that goes to zero at specific wavelengths for the given values of parameter m . In particular, increasing the order m results in QPM SHG at shorter wavelengths. Indeed, the calculated angular distribution of SH spectral intensity predicts this kind of angular behavior of the spectral intensity, as seen from Fig. 4(b). For the calculations, the following parameters were taken: the sample length 4.973 mm, the central FF wavelength 800.3 nm, the pulse duration 85 fs (FWHM), the focal spot diameter (FWHM) 80 μm , the FF incidence angle 0.6 deg, and periods of the lattice $\Lambda_x = 10$ and $\Lambda = 115.65 \mu\text{m}$ at the duty cycles of the lattice 0.73 and 0.872 ($d = 100.85 \mu\text{m}$,

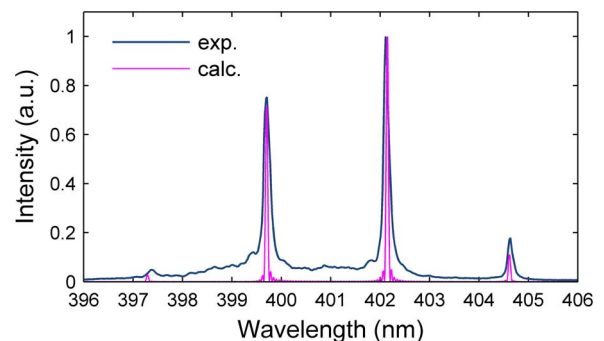


Fig. 3. Normalized measured and calculated zero-order NRND spectrum.

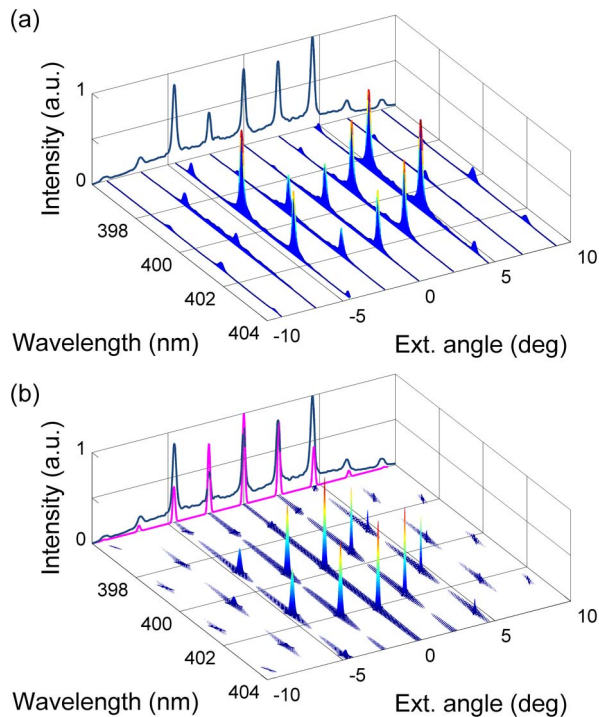


Fig. 4. (a) Measured SH spectra for specific NRND orders and (b) calculated angular distribution of SH spectral intensity. The projections are the measured (blue) and calculated (pink) angular distributions of SH intensity integrated over the spectrum. In plot (b), the SH intensities are presented in the range down to -60 dB.

$b = 14.80 \mu\text{m}$), respectively. Under these conditions, the calculated dependence provides a good description of the experimental SH spectra as to the spectral as well as angular positions of the SH peaks, while agreement between the measured and calculated amplitudes is not good enough. Nevertheless, the model proposed allows us to evaluate the SHG efficiency for specific order. For this propose, we numerically integrate Eq. (7) over the spectral and spatial frequencies. In particular, SHG efficiency for zero order was calculated to be $3\% \cdot \text{W}^{-1}$. In our opinion, the discrepancy between predicted and measured values is caused by fabrication defects of the structure and aberrations of optical system. At the same time, calculated SHG efficiency in 1D NOS of the same length ($d = \Lambda = L$) is quite low $4.5 \times 10^{-2}\% \cdot \text{W}^{-1}$. Thus we expect approximately 70 times enhancement of SHG under nonlinear Raman–Nath diffraction in 2D NLPC under study.

In summary, we have studied SHG of femtosecond laser pulses in periodic 2D NLPCs. This process is found to be in close analogy with nonlinear Raman–Nath diffraction, which takes place in 1D nonlinear photonic lattices. We derive an analytical expression for the process studied and find the theoretical results to be in good agreement with the experimental data. We estimate the enhancement factor of nonlinear Raman–Nath diffraction in 2D NLPC to be 70.

Funding. Council of the President of the Russian Federation (MK-2908.2015.2); Ministry of Education and Science of the Russian Federation (2014/7, UID RFMEFI59414X0011); Russian Foundation for Basic Research (RFBR) (13-02-01391-a, 14-02-01160-a, 15-02-03838).

Acknowledgment. The equipment of the Ural Center for Shared Use “Modern nanotechnology” UrFU was used. The authors thank A. V. Barannik for optical microscopy of the samples.

REFERENCES

1. V. Berger, Phys. Rev. Lett. **81**, 4136 (1998).
2. N. G. R. Broderick, G. W. Ross, H. L. Offerhaus, D. J. Richardson, and D. C. Hanna, Phys. Rev. Lett. **84**, 4345 (2000).
3. P. Ni, B. Ma, X. Wang, B. Cheng, and D. Zhang, Appl. Phys. Lett. **82**, 4230 (2003).
4. C. Canalias, M. Nordlöf, V. Pasiskevicius, and F. Laurell, Appl. Phys. Lett. **94**, 081121 (2009).
5. L.-H. Peng, C.-C. Hsu, J. Ng, and A. H. Kung, Appl. Phys. Lett. **84**, 3250 (2004).
6. L. Mateos, P. Molina, J. Galisteo, C. López, L. E. Bausá, and M. O. Ramírez, Opt. Express **20**, 29940 (2012).
7. Y. Zhang, J. Wen, S. N. Zhu, and M. Xiao, Phys. Rev. Lett. **104**, 183901 (2010).
8. E. Megidish, A. Halevy, H. S. Eisenberg, A. Ganany-Padowicz, N. Habshoosh, and A. Arie, Opt. Express **21**, 6689 (2013).
9. T. Ellenbogen, A. Ganany-Padowicz, and A. Arie, Opt. Express **16**, 3077 (2008).
10. T. Ellenbogen, N. Voloch-Bloch, A. Ganany-Padowicz, and A. Arie, Nat. Photonics **3**, 395 (2009).
11. N. Voloch-Bloch, K. Shemer, A. Shapira, R. Shiloh, I. Juwiler, and A. Arie, Phys. Rev. Lett. **108**, 233902 (2012).
12. A. Arie and N. Voloch, Laser Photon. Rev. **4**, 355 (2010).
13. A. Leshem, R. Shiloh, and A. Arie, Opt. Lett. **39**, 5370 (2014).
14. X.-H. Wang and B.-Y. Gu, Eur. Phys. J. B **24**, 323 (2001).
15. J. Li, Z.-Y. Li, and D.-Z. Zhang, Phys. Rev. B **77**, 195127 (2008).
16. A. Arie, N. Habshoosh, and A. Bahabad, Opt. Quantum Electron. **39**, 361 (2007).
17. B.-Q. Chen, C. Zhang, R.-J. Liu, and Z.-Y. Li, Appl. Phys. Lett. **105**, 151106 (2014).
18. S. M. Saltiel, D. N. Neshev, R. Fischer, W. Krolikowski, A. Arie, and Y. S. Kivshar, Phys. Rev. Lett. **100**, 103902 (2008).
19. S. M. Saltiel, D. N. Neshev, W. Krolikowski, A. Arie, O. Bang, and Y. S. Kivshar, Opt. Lett. **34**, 848 (2009).
20. K. Kalinowski, P. Roedig, Y. Sheng, M. Ayoub, J. Imbrock, C. Denz, and W. Krolikowski, Opt. Lett. **37**, 1832 (2012).
21. Y. Sheng, W. Wang, R. Shiloh, V. Roppo, A. Arie, and W. Krolikowski, Opt. Lett. **36**, 3266 (2011).
22. Y. Chen, W. Dang, Y. Zheng, X. Chen, and X. Deng, Opt. Lett. **38**, 2298 (2013).
23. A. M. Vyunishev, V. V. Slabko, I. S. Baturin, A. R. Akhmatkhanov, and V. Y. Shur, Opt. Lett. **39**, 4231 (2014).
24. V. Y. Shur, J. Mater. Sci. **41**, 199 (2006).
25. A. M. Vyunishev, A. S. Aleksandrovsky, A. I. Zaitsev, and V. V. Slabko, J. Opt. Soc. Am. B **30**, 2014 (2013).
26. I. V. Shutov, I. A. Ozheredov, A. V. Shumitski, and A. S. Chirkin, Opt. Spectr. **105**, 79 (2008).
27. D. H. Jundt, Opt. Lett. **22**, 1553 (1997).